X-ray Diffraction Results from Mars Science Laboratory: Mineralogy of Rocknest at Gale Crater

D. L. Bish *et al.*

X-ray Diffraction Results from Mars Science Laboratory: Mineralogy of Rocknest at Gale Crater

D. L. Bish,[1]* D. F. Blake,[2] D. T. Vaniman,[3] S. J. Chipera,[4] R. V. Morris,[5] D. W. Ming,[5]
A. H. Treiman,[6] P. Sarrazin,[7] S. M. Morrison,[8] R. T. Downs,[8] C. N. Achilles,[9] A. S. Yen,[10]
T. F. Bristow,[2] J. A. Crisp,[10] J. M. Morookian,[10] J. D. Farmer,[11] E. B. Rampe,[5] E. M. Stolper,[12]
N. Spanovich,[10] MSL Science Team†

The Mars Science Laboratory rover Curiosity scooped samples of soil from the Rocknest aeolian bedform in Gale crater. Analysis of the soil with the Chemistry and Mineralogy (CheMin) x-ray diffraction (XRD) instrument revealed plagioclase (~An57), forsteritic olivine (~Fo62), augite, and pigeonite, with minor K-feldspar, magnetite, quartz, anhydrite, hematite, and ilmenite. The minor phases are present at, or near, detection limits. The soil also contains 27 ± 14 weight percent x-ray amorphous material, likely containing multiple Fe^{3+}- and volatile-bearing phases, including possibly a substance resembling hisingerite. The crystalline component is similar to the normative mineralogy of certain basaltic rocks from Gusev crater on Mars and of martian basaltic meteorites. The amorphous component is similar to that found on Earth in places such as soils on the Mauna Kea volcano, Hawaii.

Numerous observations of the martian surface, both in situ and from orbit, suggest that basaltic soil across the planet has a fairly uniform chemical composition. Global-scale aeolian mixing of the finest grains is a major factor in this uniformity, but not too disparate basaltic compositions across the planet may also be a contributing factor (*1*, *2*). High-quality chemical data for martian soils are available from the Pathfinder, Mars Exploration Rover (MER), and Phoenix missions (*2*–*4*), and phase information has been provided through MER thermal emission and Mössbauer spectroscopic measurements (*3*, *5*–*9*). The Chemistry and Mineralogy (CheMin) instrument onboard the Mars Science Laboratory (MSL) rover Curiosity uses x-ray diffraction (XRD), which is generally the preferred and the most definitive method for determining the nature of crystalline phases (such as minerals) in solid samples. CheMin's XRD analysis on Mars coincided with the 100th-year anniversary of the discovery of XRD by von Laue (*10*).

On the basis of Alpha Particle X-ray Spectrometer (APXS) chemical analyses, the Rocknest aeolian bedform is considered to be representative of global basaltic soil at Gale crater (*11*–*13*). Curiosity delivered the <150-μm-size fraction of three samples of loose, unconsolidated material ("soil") acquired at Rocknest to the CheMin instrument inside the body of the rover, and CheMin measured two-dimensional (2D) diffraction data (Fig. 1, scoop five) for the three samples (details are available in materials and methods). Imaging shows that the soil has a range of particle sizes, 1 to 2 mm and smaller, presumably representing contributions from global, regional, and local sources (*14*). The larger particles at the top of the bedform appear to be armoring the bedform. The term soil is used here to denote any loose, unconsolidated materials that can be distinguished from rocks, bedrock, or strongly cohesive sediments. No implication of the presence or absence of organic materials or living matter is intended, nor is the genesis of the deposit inferred.

Results

Crystalline Components

Initial analyses of the measured diffraction data from three different scoops revealed the presence of plagioclase feldspar, forsteritic olivine, augite, and another pyroxene, with no evidence of any phyllosilicate mineral. Rietveld refinements including numerous candidate phases revealed the presence of pigeonite with augite. Refinements using augite with orthopyroxene or clinopyroxene were inferior to an augite-pigeonite model. A single-plagioclase model was as good as a model with two plagioclases of different composition

(such as different unit-cell parameters or Na-Ca site occupancies), so only a single plagioclase was used. However, we cannot exclude the presence of multiple or zoned pyroxene, olivine, and plagioclase compositions. Refinements also clarified the minor mineral species and their abundances and allowed exclusion of many possible minerals. The presence of minor phases was evaluated individually by including each in the model and evaluating their effect on the fit (Fig. 2). All three scoop samples produced similar results, although changes in the XRD pattern for scoop three as a function of time suggested that sample was ejected from the XRD sample cell by vibration, and these data were not used. The 2σ values given in Table 1 are from the Rietveld refinement; they show that several minor phases are questionable, with errors close to or exceeding the refined values. Refined unit-cell parameters for the major phases (Table 2) were used to estimate the compositions of these phases by comparison with literature values (*15*). Such comparisons gave $(Mg_{0.62(3)}Fe_{0.38})_2SiO_4$ for the composition of the olivine mineral (parenthetical numbers in the subscripts refer to standard errors from fits of our unit-cell parameters to literature values and do not consider the errors on refined unit-cell parameters). This composition agrees well with the refined Mg-Fe site occupancies, $(Mg_{0.64(3)}Fe_{0.36})_2SiO_4$. The plagioclase unit-cell parameters gave a composition of $(Ca_{0.57(13)}Na_{0.43})(Al_{1.57}Si_{2.43})O_8$, which does not agree with the refined site-occupancy data (close to the Na end-member composition). We consider the unit-cell parameter trends to be more reliable than the site occupancy information, which is based on diffracted intensities over the short angular range (<55° 2θ) provided by CheMin. In addition, diffraction intensities may have been affected by preferred crystallite orientation. Although we did not use a preferred orientation correction in our
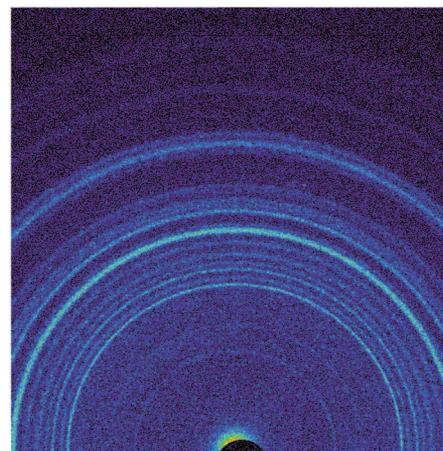

Fig. 1. CheMin 2D XRD pattern of scoop 5, representing 26.9 hours of integration time. Image contrast has been enhanced and colorized to emphasize the Debye diffraction rings. The black semicircle at the bottom is the shadow of the beam stop.

[1]Department of Geological Sciences, Indiana University, Bloomington, IN 47405, USA. [2]NASA Ames Research Center, Moffett Field, CA 94035, USA. [3]Planetary Science Institute, Tucson, AZ 85719, USA. [4]Chesapeake Energy, Oklahoma City, OK 73154, USA. [5]NASA Johnson Space Center, Houston, TX 77058, USA. [6]Lunar and Planetary Institute, Houston, TX 77058, USA. [7]In-Xitu, Campbell, CA 95008, USA. [8]Department of Geology, University of Arizona, Tucson, AZ 85721, USA. [9]Engineering and Science Contract Group/United Technologies Corporation Aerospace Systems, Houston, TX 77058, USA. [10]Jet Propulsion Laboratory/California Institute of Technology, Pasadena, CA 91109, USA. [11]Department of Geological Sciences, Arizona State University, Tempe, AZ 85287, USA. [12]California Institute of Technology, Pasadena, CA 91125, USA.

*Corresponding author. E-mail: bish@indiana.edu
†MSL Science Team authors and affiliations are listed in the supplementary materials.

Fig. 2. Rietveld refinement results for scoop 5 (final R_{wp} = 4.3%; R_{wp} = weighted profile residual from the Rietveld refinement). Observed (blue) versus calculated (red) pattern, with difference curve (obs-calc) at the bottom (gray). The difference peak at ~25.6° 2θ is due to scattering from the aluminum light shield. Minerals included in the refinement model are listed in Table 1.

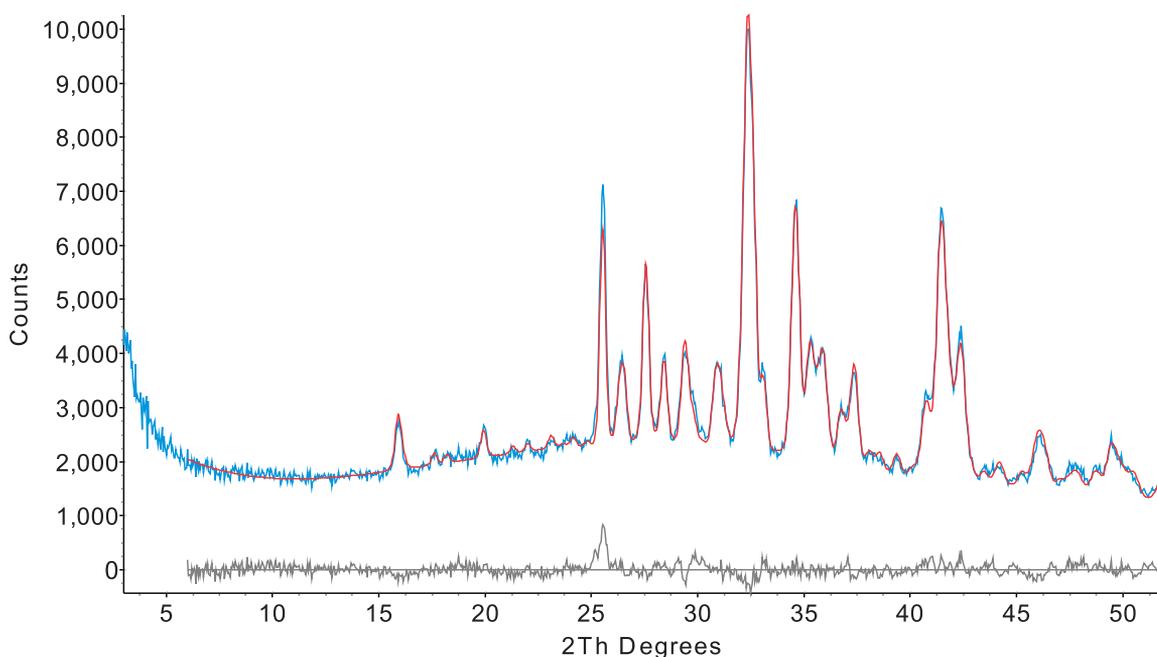## Table 1. Crystalline components (amorphous-free, normalized to 100%) of the Rocknest scoop 5 soil.

Mineral	Weight (%)	2σ (%)
Plagioclase (~An57)	40.8	2.4
Forsterite (~Fo62)	22.4	1.9
Augite	14.6	2.8
Pigeonite	13.8	2.8
Magnetite	2.1	0.8
Anhydrite	1.5	0.7
Quartz	1.4	0.6
Sanidine*	1.3	1.3
Hematite*	1.1	0.9
Ilmenite*	0.9	0.9

*At or near detection limit

final refinements, we did see indications of minor orientation effects in the data, as evidenced by small improvements in Rietveld fits when a preferred orientation correction was used for plagioclase. Refined unit-cell parameters for pigeonite gave a composition of $(Mg_{1.13}Fe_{0.68}Ca_{0.19})Si_2O_6$, compared with octahedral site-occupancy refinement results of $(Mg_{1.71(15)}Fe_{0.13}Ca_{0.16})Si_2O_6$. Refined unit-cell parameters for augite gave a composition of $(Mg_{0.88(10)}Fe_{0.37}Ca_{0.75(4)})Si_2O_6$, which is broadly consistent with octahedral site-occupancy refinement results of $(Mg_{0.58(15)}Fe_{0.71}Ca_{0.71})Si_2O_6$. Unit-cell parameters suggest atomic Mg:Fe ratios for augite and pigeonite of 2.4 and 1.7, respectively. Comparable ratios imply the two pyroxenes originated from the same magma, rather than having experienced post-crystallization alteration (such as pigeonite inversion) or being from different source regions [16].

We also evaluated the presence of a variety of Ca-, K-, Fe- and Mg-sulfates; halides; Ca-, Mg-, and Fe-carbonates; phosphates; and Ca- and Mg-perchlorates (many of these hydrated). It is straightforward to include each of these phases in the Rietveld model and evaluate its potential contribution to the diffraction pattern, both visually and based on the fit parameter (R_{wp}). Using this approach, we found no evidence for the presence of any of these phases, other than those listed in Table 1, several of which have 2σ uncertainties greater than the refined abundances. If halides, perchlorates, carbonates, phosphates, or other sulfate phases are present as crystalline phases, they are below the detection limits of the CheMin instrument [1 to 2 weight percent (wt %)]. Although data from the Sample Analysis at Mars (SAM) instrument suite suggest the presence of a small amount of perchlorate (0.3 to 0.5 wt %) in the Rocknest soil [17, 18], models that included Mg-perchlorate·6H$_2$O and Ca-perchlorate·4H$_2$O refined to 0 wt % for these phases; thus, we find no diffraction evidence for either of these phases.

Amorphous or Poorly Ordered Components

The elevated background in the 15 to 40° 2θ range in Fig. 2 results from the presence of one or more amorphous or poorly ordered components. The low-angle background is also elevated significantly above that seen with empty cells. Hence, we also analyzed the CheMin XRD data using a modified version of the FULLPAT program [19], which allows direct determination of the abundance of amorphous components. The FULLPAT analyses explicitly used patterns for both ordered and amorphous phases, and the entire diffraction patterns, including background, were fit. The abundances of crystalline and amorphous phases (Table 3) were normalized to sum to 100 wt % in accordance with the adiabatic method [20], and scoops four and five gave an average amorphous content of 27 wt %. The uncertainty on individual amorphous values may be as high as 50 wt % relative. Of the amorphous standards included in the analysis, only one allophane and a basaltic glass gave positive concentrations. The materials used as standards for amorphous materials were chosen as reasonable representatives of expected materials in the Mars aeolian bedform. However, the exact nature of the amorphous component remains unclear. Although a synthetic SO$_3$- and Cl-free Gusev-composition basaltic glass was the dominant amorphous component in our FULLPAT fit, it may be just one of many amorphous components that have similar XRD patterns, and these analyses do not unambiguously identify the amorphous component (or components). Similarly, allophane may be an XRD surrogate for another amorphous phase such as the Fe^{3+}-bearing phase hisingerite, and the sample may contain a small amount of such material.

The Rocknest soil contains glassy-luster spherules that may have an impact or pyroclastic origin [21], but our results do not necessarily indicate that the amorphous component in Rocknest soil is dominated by basaltic glass; other observations suggest otherwise. MER Mössbauer analyses of basaltic soils from Gusev and Meridiani show substantial abundances of an amorphous phase containing Fe^{3+} [generically referred to as nanophase ferric oxide (npOx)] [7], and taken together, the MSL CheMin and SAM data suggest that the Gusev amorphous phase (or phases) is volatile rich (containing, for example, H$_2$O/OH or SO$_3$) [18]. The abundances (Table 1) and chemistry (from unit-cell parameters) of the crystalline phases identified by CheMin, coupled with mass-balance considerations from APXS analyses of Rocknest soil, suggest that the amorphous component is SO$_3$- and Cl-bearing [11, 22]. Last, if MER-like levels of Fe^{3+} are present in Rocknest soil, then the amorphous component must also be the carrier of the Fe^{3+} (with the exception of

Table 2. Refined unit-cell parameters for major crystalline phases in the Rocknest soil (scoop five).

Mineral	Unit-cell parameter	Value (ESD)
Forsterite	a (Å)	10.327 (7)
	b (Å)	6.034 (7)
	c (Å)	4.771 (5)
Plagioclase	a (Å)	8.177 (6)
	b (Å)	12.868 (9)
	c (Å)	7.113 (5)
	α (degrees)	93.43 (4)
	β (degrees)	116.26 (2)
	γ (degrees)	90.13 (3)
Pigeonite	a (Å)	9.652 (9)
	b (Å)	8.92 (1)
	c (Å)	5.254 (7)
	β (degrees)	108.0 (1)
Augite	a (Å)	9.782 (9)
	b (Å)	8.939 (9)
	c (Å)	5.269 (7)
	β (degrees)	106.25 (9)

Table 3. Amorphous contents (wt %) from FULLPAT analyses of scoops 4 and 5.

	Scoop 4	Scoop 5
Gusev-composition basaltic glass	23	25
Allophane-like material	3	2
Total	26	27

magnetite and possible hematite) that is responsible for the reddish color of the soil (*14, 22*). We did not have access to a pure sample of npOx for use as a standard in FULLPAT analyses and cannot exclude this from the amorphous phase inventory in these samples.

Discussion

Our XRD data reveal a rich inventory of crystalline and amorphous phases in Rocknest soil and provide insight into chemical and physical weathering processes on Mars. The crystalline component is dominated by plagioclase, olivine, augite, and pigeonite, which is consistent with and confirms a variety of previous orbital and lander analyses (*2, 3, 5–9*). This assemblage, particularly the Fe-rich forsterite and the presence of a substantial amorphous component, is consistent with limited aqueous alteration, similar to conclusions from the Phoenix lander (*23*). We found no XRD evidence for zeolite minerals, which were previously proposed (*24*) as an alternative to feldspar in martian dust. CheMin is sensitive to the presence of zeolite minerals because their major diffraction peaks lie in an angular range with few or no other peaks. The presence of pigeonite and the similarity of the augite and pigeonite Fe:Mg ratios imply that the crystalline component results from the near-surface crystallization of basaltic lavas as opposed to formation in plutonic rocks. The crystalline component is

very similar to normative basalt mineralogies calculated from Gusev APXS data (*25*) and is also qualitatively similar to mineralogies of martian basaltic meteorites (*16*). Although hydrous phyllosilicates (such as smectites) have been identified on the martian surface through orbital spectral data, the XRD data did not reveal any phyllosilicate in this soil. The absence of smectites is somewhat surprising because orbital spectral data suggest the presence of smectites in and around Gale crater (*26*). Because diffraction peaks from typical phyllosilicates (such as smectites) generally are quite broad, our detection limits for such minerals are comparatively poor, probably on the order of at least 5%. The lack of any detectable hydrated crystalline phase is important, as is the lack of detectable crystalline sulfate (other than minor anhydrite), perchlorate, or chloride phases. This result, coupled with the observation with the SAM instrument of volatile evolution (*18*), implies that virtually the entire volatile inventory of the Rocknest soil is associated with the amorphous component, an important detail that previous investigations were unable to detect. By combining these quantitative XRD results with compositional estimates from unit-cell parameters and bulk chemistry, it has been possible to determine the chemical compositions of the major phases, including that of the amorphous component (or components) (*11*). With the exception of the S content, the amorphous component (or components) are remarkably similar to those found on Earth in volcanic soils, such as those on the flanks of Mauna Kea volcano, Hawaii (*27*). The CheMin XRD results should be applicable to previous and future soil measurements on Mars because soil compositions from many different measurements at several locales appear so similar (*28*). In addition, these data provide critical ground-truth information on martian soils and expand our understanding of the fine-grained component on the martian surface.

Materials and Methods

Samples and Measurements

Scoops three, four, and five of the soil were introduced into the Collection and Handling for In situ Martian Rock Analysis (CHIMRA) sample processing system on *Curiosity*. Each scoop sample was passed through a 150-μm sieve (thus excluding the coarser-grained material visible in images of the bedform) before delivering a portion to the CheMin inlet funnel. Scoops one and two were used to clean the CHIMRA system and were not introduced into *Curiosity*'s instruments.

Scoops three and four were placed into a sample cell with 10-μm-thick Kapton (Dupont, Wilmington, Delaware) windows, and scoop five was placed into a cell with 6-μm-thick Mylar (Dupont, Wilmington, Delaware) windows. Both types of cells have the potential to contribute broad scattering signatures to the diffraction patterns.

In addition, an aluminized light shield also contributes "peaks" to the observed diffraction patterns. Kapton contributes a broad peak centered at ~15 Å, whereas Mylar has a very small amount of scattering at low angles. Mylar cells are therefore preferred when searching for diffraction signatures from phyllosilicates or other materials having diffraction peaks at low angles. Only ~10 mm^3 of material is required to fill the active portion of the sample cell, which is a disc-shaped volume 8 mm in diameter and 175 μm thick. The collimated ~70 μm diameter x-ray beam illuminates the center of the sample cell. A piezoelectric vibration system on each cell shakes the material during analysis, causing all of the grains in the cell to pass through the x-ray beam in random orientations over the time course of an analysis.

CheMin measures XRD and x-ray fluorescence (XRF) data simultaneously using Co radiation in transmission geometry (*29*). The instrument operates in single-photon counting mode so that the majority of CCD pixels are struck between each readout by either a single x-ray photon or by no photons. In this way, the system can determine both the energy of the photons striking the CCD (XRF) and the 2D position of each photon (XRD) (*29*). The energy and positional information of detected photons in each frame are summed over repeated 10-s measurements into a "minor frame" of 30 min of data (180 frames). CheMin collects as many minor frames as possible for the available analysis time, which is usually five to seven per night, and these are summed to create one data file for each night of data collection. The 2D distribution of Co Kα x-ray intensity represents the XRD pattern of the sample (Fig. 1), and circumferential integration of these rings, corrected for arc length, produces a conventional 1D XRD pattern. CheMin generally operates for only a few hours each night during which time the CCD is at its lowest temperature. Thus, XRD data were acquired over multiple nights for each scoop sample to provide acceptable counting statistics. Data were measured for 3.8 hours (scoop 3), 15.7 hours (scoop 4), and 26.9 hours (scoop 5). The data for individual minor frames and for each night's analyses were examined separately, and there was no evidence of any changes in instrumental parameters as a function of time over the duration of these analyses. Before analysis of each new scoop, measurements were made of the empty cell to confirm that it was indeed empty before receiving the sample. We calibrated the flight instrument on the ground before flight using a quartz-beryl standard, and measurement of this standard on Mars showed no changes in instrument geometry or dimensions.

Crystalline Components

All XRD data were first evaluated by comparisons and searches of the International Centre for Diffraction Data (ICDD) Powder Diffraction File using Bruker AXS DIFFRAC.EVA (Bruker AXS, Karlsruhe, Germany, 2000) and MDI Jade (Materials Data Incorporated, Livermore, California)

software packages, which revealed the presence of plagioclase feldspar, forsteritic olivine, augite, and another pyroxene. There was no evidence of any phyllosilicate, which would have produced diffraction peaks at low angles (5 to 15° 2θ). The comparatively large instrumental peak widths for the CheMin instrument (~0.3° 2θ full-width at half-maximum at 25° 2θ) limited our ability to determine accurately the presence of minor crystalline phases (<3 wt %). The data were analyzed further via Rietveld methods, using Topas (Bruker AXS, 2000). We used the fundamental-parameters approach within Topas, along with additional convolutions, to model the experimental profiles. We also used an emission spectrum including Co Kα, with a refinable Co Kβ component. The Rietveld method involves constructing a model consisting of the crystal structures of all component phases, and the differences between the observed and simulated diffraction patterns are minimized by varying components of the model, including scale factors (related to phase abundance), unit-cell parameters, and crystallite-size and strain broadening parameters for each phase. Atomic positions and site occupancies were generally not varied, although octahedral site occupancies were varied for forsteritic olivine, augite, and pigeonite, and Na-Ca occupancies were varied for the plagioclase component. This method thus provides information on all well-ordered phases (crystalline phases), but it is not directly applicable to disordered phases such as clay minerals or amorphous components.

Amorphous or Poorly Ordered Components

FULLPAT operates on the principle that diffraction and scattering patterns for all phases in a sample are additive. By fitting full diffraction patterns—including the background, which contains important information on sample composition and matrix effects—explicit analysis of amorphous or partially ordered materials can often be readily accomplished if the amorphous/disordered phases are included in the analyses as distinct phases. Thus, FULLPAT allows direct analysis of the abundance of amorphous components, rather than determining them as the difference from 100 wt % in an internal standard quantitative analysis. Like all full-pattern fitting methods, accurate analysis requires representative standards or structure models. A large variety of pure mineral standards, disordered materials (allophanes, ferrihydrite, and aluminosilicate gels), and a synthetic basaltic glass of Gusev composition were measured. Each of these was run as a pure phase and was also mixed with a beryl standard in a 50:50 weight ratio to determine a reference intensity ratio (RIR) for subsequent use in FULLPAT (*30, 31*). All standard data were measured on a CheMin IV instrument at the NASA Johnson Space Center; the CheMin IV instrument geometry is very similar to the instrument on MSL and is considered a good proxy for the flight instrument. Peak areas for each phase were compared against the intensity of the beryl 100 reflection, and the measured beryl RIR of 1.70 relative to corundum (measured on a laboratory instrument) was used to convert the RIR(beryl) to the conventional RIR(corundum) value. During FULLPAT analysis, the intensity of each standard pattern was normalized to the intensity of a pure pattern of corundum used as datum. Thus, using this corundum datum 113 reflection intensity and the measured RIR for each standard phase, the pattern of each disordered phase could be normalized to the appropriate overall intensity based on its measured intensity area used for RIR determination.

Because few standard data for pure phases have been measured on the CheMin flight instrument, an alternate method for calculating standard data representative of the MSL CheMin instrument was often used. This process involved first determining instrumental peak shapes and widths as function of 2θ by using the beryl standard measured on the MSL instrument. We then calculated diffraction patterns for each standard using the appropriate crystal structure information and the instrumental profiles determined above for Co Kα radiation. The final step in calculation of standard data for FULLPAT was to normalize the intensity of the calculated pattern to the corundum datum pattern by using the calculated RIR as outlined above. The scaled measured and calculated library patterns, for both ordered and amorphous phases, were then used with FULLPAT.

References and Notes

1. B. C. Clark *et al.*, Chemical-composition of martian fines. *J. Geophys. Res.* **87**, 10059–10067 (1982). doi: 10.1029/JB087iB12p10059

2. R. Gellert *et al.*, Chemistry of rocks and soils in Gusev Crater from the alpha particle x-ray spectrometer. *Science* **305**, 829–832 (2004). doi: 10.1126/science.1099913; pmid: 15297665

3. A. S. Yen *et al.*, An integrated view of the chemistry and mineralogy of martian soils. *Nature* **436**, 49–54 (2005). doi: 10.1038/nature03637; pmid: 16001059

4. M. H. Hecht *et al.*, Detection of perchlorate and the soluble chemistry of martian soil at the Phoenix lander site. *Science* **325**, 64–67 (2009). pmid: 19574385

5. I. O. McGlynn, C. M. Fedo, H. Y. McSween Jr., Soil mineralogy at the Mars Exploration Rover landing sites: An assessment of the competing roles of physical sorting and chemical weathering. *J. Geophys. Res.* **117**, E01006 (2012). doi: 10.1029/2011JE003861

6. H. Y. McSween Jr., I. O. McGlynn, A. D. Rogers, Determining the modal mineralogy of Martian soils. *J. Geophys. Res.* **115**, E00F12 (2010). doi: 10.1029/2010JE003582

7. R. V. Morris *et al.*, Mössbauer mineralogy of rock, soil, and dust at Gusev Crater, Mars: Spirit's journey through weakly altered olivine basalt on the Plains and pervasively altered basalt in the Columbia Hills. *J. Geophys. Res.* **111**, E02S13 (2006). doi: 10.1029/2005JE002584

8. R. V. Morris *et al.*, Mineralogy at Gusev crater from the Mossbauer spectrometer on the Spirit rover. *Science* **305**, 833–836 (2004). doi: 10.1126/science.1100020; pmid: 15297666

9. P. R. Christensen *et al.*, Mineralogy at Meridiani Planum from the Mini-TES Experiment on the Opportunity Rover. *Science* **306**, 1733–1739 (2004). doi: 10.1126/science.1104909; pmid: 15576609

10. M. Eckert, Max von Laue and the discovery of x-ray diffraction in 1912. *Ann. Phys.* **524**, A83–A85 (2012). doi: 10.1002/andp.201200724

11. R. V. Morris *et al.*, presented at the 44th Lunar and Planetary Science Conference, March 2013, abstract 1653; published on CD by the Lunar and Planetary Institute, Houston, TX (2013).

12. A. S. Yen *et al.*, presented at the 44th Lunar and Planetary Science Conference, March 2013, abstract 2495; published on CD by the Lunar and Planetary Institute, Houston, TX (2013).

13. R. Gellert *et al.*, presented at the 44th Lunar and Planetary Science Conference, March 2013, abstract 1432; published on CD by the Lunar and Planetary Institute, Houston, TX (2013).

14. D. F. Blake *et al.*, Curiosity at Gale crater, Mars: Characterization and analysis of the Rocknest sand shadow. *Science* **341**, 1239505 (2013).

15. S. M. Morrison *et al.*, presented at the 44th Lunar and Planetary Science Conference, March 2013, abstract 1831; published on CD by the Lunar and Planetary Institute, Houston, TX (2013).

16. A. H. Treiman *et al.*, presented at the 44th Lunar and Planetary Science Conference, March 2013, abstract 1113; published on CD by the Lunar and Planetary Institute, Houston, TX (2013).

17. P. D. Archer Jr. *et al.*, presented at the 44th Lunar and Planetary Science Conference, March 2013, abstract 2168; published on CD by the Lunar and Planetary Institute, Houston, TX (2013).

18. L. A. Leshin *et al.*, Volatile, isotope, and organic analysis of martian fines with the Mars Curiosity rover. *Science* **341**, 1238937 (2013).

19. S. J. Chipera, D. L. Bish, FULLPAT: A full-pattern quantitative analysis program for x-ray powder diffraction using measured and calculated patterns. *J. Appl. Cryst.* **35**, 744–749 (2002). doi: 10.1107/S0021889802017405

20. F. H. Chung, Quantitative interpretation of x-ray diffraction patterns of mixtures. II. Adiabatic principle of x-ray diffraction analysis of mixtures. *J. Appl. Cryst.* **7**, 526–531 (1974). doi: 10.1107/S0021889874010387

21. R. Yingst *et al.*, presented at the 44th Lunar and Planetary Science Conference, March 2013, abstract 1257; published on CD by the Lunar and Planetary Institute, Houston, TX (2013).

22. D. F. Blake *et al.*, presented at the 44th Lunar and Planetary Science Conference, March 2013, abstract 1289; published on CD by the Lunar and Planetary Institute, Houston, TX (2013).

23. W. T. Pike *et al.*, Quantification of the dry history of the Martian soil inferred from in situ microscopy. *Geophys. Res. Lett.* **38**, L24201 (2011). doi: 10.1029/2011GL049896

24. S. W. Ruff, Spectral evidence for zeolite in the dust on Mars. *Icarus* **168**, 131–143 (2004). doi: 10.1016/j.icarus.2003.11.003

25. D. W. Ming *et al.*, Geochemical and mineralogical indicators for aqueous processes in the Columbia Hills of Gusev crater, Mars. *J. Geophys. Res. Planets* **111**, E02S12 (2006). doi: 10.1029/2005JE002560

26. R. E. Milliken, J. P. Grotzinger, B. J. Thomson, Paleoclimate of Mars as captured by the stratigraphic record in Gale Crater. *Geophys. Res. Lett.* **37**, L04201 (2010). doi: 10.1029/2009GL041870

27. R. V. Morris *et al.*, Phyllosilicate-poor palagonitic dust form Mauna Kea Volcano (Hawaii): A mineralogical analogue for magnetic martian dust? *J. Geophys. Res.* **106**, 5057–5083 (2001). doi: 10.1029/2000JE001328

28. R. Gellert *et al.*, Alpha Particle X-Ray Spectrometer (APXS): Results from Gusev crater and calibration report. *J. Geophys. Res.* **111**, E02S05 (2006). doi: 10.1029/2005JE002555

29. D. Blake *et al.*, Characterization and calibration of the CheMin mineralogical instrument on Mars Science Laboratory. *Space Sci. Rev.* **170**, 341–399 (2012). doi: 10.1007/s11214-012-9905-1

30. C. N. Achilles, R. V. Morris, S. J. Chipera, D. W. Ming, E. B. Rampe, presented at the 44th Lunar and Planetary Science Conference, March 2013, abstract 3072; published

on CD by the Lunar and Planetary Institute, Houston, TX (2013).

31. E. B. Rampe *et al.*, presented at the 44th Lunar and Planetary Science Conference, March 2013, abstract 1188; published on CD by the Lunar and Planetary Institute, Houston, TX (2013).

Supplementary Materials
www.sciencemag.org/content/341/6153/1238932/suppl/DC1
MSL Science Team Author List